Hybrid Energy-Based and Bayesian Statistical Inference Fatigue Life Prediction of AM Components

Dino Celli*, **Justin Warner**, **Lucas Smith**, **Luke Sheridan**, **Onome Scott-Emuakpor**

*Air Force Research Laboratory
2066 5th St.
WPAFB OH, 45324
USA

dino.celli.1@us.af.mil

Keywords: Research Symposium, Fatigue Life Prediction, Strain-Energy, Bayesian Statistical Inference

ABSTRACT

A fatigue life prediction method is proposed which can concurrently approximate both SN behaviour as well as the inherent variability of fatigue efficiently via a novel combination of a Two-Point energy-based life prediction tool and Bayesian statistical inference. The purpose of such a tool is for the quality assessment and verification of components using Additive Manufacturing (AM) processes and other materials with a limited knowledgebase. The variability in fatigue life of AM components often stem from undesirable microstructure or, more commonly, internal defects onset by suboptimal process parameters. Satisfactory process parameters and post heat-treatments have shown to mitigate undesirable fatigue characteristics but determination of optimal parameters for the build process can be an extensive and costly endeavour due to either a limited knowledgebase or proprietary restrictions. Therefore, the proposed life prediction method enables determination of fatigue performance of a material with little or no prior information of the material and a limited number of experimental tests. Validation data sets of AM laser powder bed fusion Inconel 718 and Ti-6Al-4V EBM as well as conventionally manufactured Aluminum 6061 are considered. This is performed by simulating fatigue data for LCF and HCF using a simplistic energy-based fatigue life prediction method, or Two Point method, to formulate prior distributions of RFL model parameters. SN life prediction curves are evaluated using Bayesian statistical inference and stochastic sampling techniques for distribution estimation and carried out in a dynamic way such that the life prediction model is continually updated with the generation of new experimental data.

1.0 INTRODUCTION

Interest in AM has grown beyond an expeditious process for prototyping and is now being viewed as a viable option toward small to medium scale production of end-use product fabrication as well as repair. Current research on AM costs, when compared to contemporary fabrication processes, have shown promise that the AM process may become more cost effective, while simultaneously reducing lead times of component fabrication, on small to medium scale production (Thomas, 2014). These advantages are primarily due to the fabrication of components beginning directly with the release of a design, as opposed to awaiting further tooling, and reducing material waste. Making direct cost comparison remains challenging due to the complexity associated with each AM process in addition to the field not yet having reached maturity (Atzani, 2012).

A number of AM technologies are ideal for retrofitting and repair of equipment and components that are no longer supported by vendors either as a result of outdated components or the vendor no longer existing. Specifically, PBF and DED have demonstrated significant utility for the repair, refurbishment, and retrofit for

GTE blades and other critical aerospace components (Scott-Emuakpor, 2021; Leino, 2016; Raju, 2015; Optomec, 2015). This provides a tremendous benefit to the sustainability of long service duration equipment or, in some cases, equipment that has exceeded its originally designed life cycle. With this in mind, the advantage of AM continues to hold the interest of many industries. The aerospace industry is no exception but presents unique challenged due to rigorous safety standards and regulations.

Extensive fatigue testing is still required to fully characterize the stochastic nature of fatigue. This is compounded when considering AM and build-to-build variation with the manipulation or optimization of process parameters. For conventionally wrought material, 40 or more fatigue tests are recommended for a full statistical representation of fatigue performance for one operational environment and 5-11 tests at one simulated operating condition to understand mean and variation of fatigue performance (Schneider, 2003; Manchin, 1984). For example, 45 specimens would be conducted at only one temperature condition, environment (e.g. standard laboratory conditions or flow path in GTE), stress ratio, direction of loading. When considering the operational environment and stress state a GTE blade may be subjected to, the blocking of experiments begins to rapidly increase.

Currently, powder bed fusion (PBF) is one of the most common AM processes for the fabrication of metallic components. PBF is the process of building a component by selectively fusing metallic powder layer-by-layer, starting from a build plate. As previously stated, a variety of PBF techniques exist encompassing: direct metal laser sintering (DMLS), electron beam melting (EBM), and others such as selective laser melting. It has become understood in the field of metal AM that process parameter selection is critical to the resultant mechanical and fatigue properties of the final build. With sub-optimal process parameters, AM components can be produced with defects such as surface roughness, unmelted or partially fused powder, and isolated or clustered porosity leading to highly variable mechanical and fatigue performance. Similar to most other AM processes, PBF has many key process parameters. The primary PBF parameters include energy density, laser power, hatching speed, scan strategy, layer thickness, recycled versus virgin powder, and object geometry. For this reason, much industrial and scientific interest has been directed towards the fabrication of objects defect-free or near-defect free through the optimization and manipulation of process parameter (Jared, 2015; Salem, 2016; Verma, 2019). Although with approximately 30 key process parameters or more, optimization of process parameters for any one build geometry can be a formidable task and typically requires rigorous analysis of fatigue performance; in turn, it is an exceedingly time consuming and costly task (Mani, 2015).

Presented in this paper is a fatigue life prediction framework that combines the Two Point energy method with Bayesian statistical inference and parameter estimation for the purposes of rapidly approximating stress vs. cycle to failure and S-N fatigue life prediction. The method developed utilizes the inherent variation of fatigue and strain-energy dissipation via the Two Point energy-based life prediction method. Then, a Bayesian update is performed with the observed data concurrently in an effort to obtain a robust fatigue life prediction methodology. The methodology described accurately predicts HCF life with LCF data to accelerate experimental testing with limited resources. Specifically, the main advantage of this process obtains the aforementioned desires with a limited number of LCF data points, and this process is beneficial to AM materials that may exhibit significantly different fatigue properties than conventionally wrought material or with different process parameters. The benefit of this methodology is demonstrated by first discussing a large data set of conventional Al6061-T6 extruded rod. Then, the life prediction framework is performed for AM for Inconel 718 specimens followed by EBM Ti 6Al-4V to demonstrate this methods ability to evaluate the potential of a material before the need for significant time and monetary investment to characterize the material.

2.0 BACKGROUND AND THEORY

2.1 Energy-Based Fatigue Life Prediction

The fundamental concept of energy-based fatigue life prediction is the assumption that, for a given material, there exists a critical and constant amount of energy that will cause fatigue fracture. These approaches include the monitoring of acoustic emissions, entropy degradation, and strain-energy. For strain-energy based approaches, prediction is determined by introducing the hypothesis that under cyclic loading, failure will occur when the total cumulative dissipated strain energy density (SED) via plastic work or damage reaches the critical energy. Ideally, if this critical energy to failure is known and the strain energy dissipation rate can be measured or approximated, the fatigue life of a component can then be determined (Feltner, 1961; Stowell, 1969; Scott-Emuakpor, 2004; and Scott-Emuakpor 2010).

The use of strain energy, and specifically SED as a critical damage parameter was proposed as early as the 1920's, relating SED dissipated per cycle to the number of cycles to failure (Jasper, 1923; Enomoto, 1955). To define SED, a representative hysteresis loop is presented in Figure 1. For fatigue, this hysteresis loop is assumed to start at a state of zero stress and undergo a tensile loading to a maximum value of stress. Then the loading is reversed to minimum value of stress and finally unloaded back to zero stress. For purely elastic deformation, this hysteresis loop will be a straight line. However, if we assume plastic deformation or damage occurs, then the area within the hysteresis loop will be finite. This finite area is then defined as W_d or the SED dissipated per cycle. If the critical amount of energy and W_d for a given operating condition are both defined, then fatigue failure can be predicted.

SED is often viewed as a favorable damage parameter for several reasons. First, strain energy is a scalar quantity and intrinsically represents damage done to the material system subjected to a single axis or multi-axis loading. As well for some materials, the critical energy to cause fatigue failure W_f has been shown to be equivalent to the total SED dissipated for tensile fracture W_m. This is highly advantageous as W_m can be found quickly from a monotonic tensile test and fatigue prediction can be quickly evaluated with a cyclic plasticity model. Despite the systematic variation of W_f in the VLCF regime, strain-energy fatigue life prediction methods have still demonstrated the ability to predict fatigue life of both LCF and HCF SN behavior for Aluminum 6061, Titanium 6Al-4V, and IN 718 (Scott-Emuakpor, 2007; Scott-Emuakpor, 2010; Ozaltun, 2009; Holycross, 2015; Celli, 2017; Celli, 2020). The work in this document attempts to circumvent the extensive task of fully characterizing the underlying phenomenon which causes the variation of W_f with respect to in the LCF region utilizing both stochastic sampling techniques and Bayesian statistical inference combined with the Two-Point energy-based life assessment method.

The ``Two-Point'' energy-based life assessment method, proposed by Shen and Akanda (2015), is utilized in this study as a method to determine multiple fatigue life predictions as well as approximating inherent SN variation. As previously stated, energy-based methods, including the Two-Point method, rely on the assumption that fatigue failure occurs once a critical amount of strain energy has been exhausted. To model W_d, the Ramberg-Osgood plasticity model is presented with the cyclic strength coefficient and strain hardening exponent K' and n'. The Two-Point method assumes that the dissipated cyclic SED (W_d) is a constant value for a given stress amplitude (σ_a) and the total SED dissipated (W_f) is a constant value for all σ_a. Therefore, the method requires that the experimental cycles and SED to failure N_f and W_f at defined stress amplitudes σ_a are known. If it is assumed that W_f is constant for all σ_a, then fatigue life can be quickly predicted by determining an expression for W_d.

The Two-Point method has shown to provide accurate fatigue life prediction for stress ranges bounded within the two stress amplitudes considered and assuming the SN behavior bounded by the two points is approximately linear in log-log space. Proposed by Shen and Akanda (2015 and 2016), the derivation begins

similar to common definitions of energy-based fatigue life predictions. First the total strain range is separated into elastic and plastic components,

$$\Delta\epsilon = \Delta\epsilon_e + \Delta\epsilon_p \tag{1}$$

where $\Delta\epsilon$ represents the total strain range and set equivalent to summation of the elastic and plastic strain range components $\Delta\epsilon_e$ and $\Delta\epsilon_p$ respectively. The elastic component of strain is described by Young's modulus E in Eqn (2).

$$\Delta\epsilon_{\mathrm{e}} = \frac{\Delta\sigma}{\mathrm{E}} \tag{2}$$

For the plastic relationship, numerous models have been proposed in an attempt to fully describe the phenomenon of plastic deformation and the many influencing parameters of plasticity including strain rate and temperature dependencies. However, the Ramberg-Osgood cyclic parameters are presented here for the simplicity of the two-parameter power-law model as well as the ability in doing so to generate simulated data points. The relationship is shown in Eqn (3) where K' represents the cyclic strength coefficient and n' is the strain hardening exponent.

$$\Delta\epsilon_p = \frac{\Delta\sigma^{\frac{1}{n'}}}{K'} \tag{3}$$

Substituting Eqn (2) and (3) into Eqn (1) yields Eqn (4), the Ramberg-Osgood (RO) model. This can be seen schematically in Figure 1. Note that the origin in Figure 1 has been shifted to the minimum ϵ and σ point for mathematical convenience.

$$\Delta\epsilon = \frac{\Delta\sigma}{E} + \left(\frac{\Delta\sigma}{K'}\right)^{\frac{1}{n'}} \tag{4}$$

With Eqn (4) defined, the cyclic SED can now be calculated as the area within the hysteresis as a component undergoes fatigue. First, the material is assumed to be isotropic or the elastic-plastic tensile loading behavior is equivalent to the compressive load behavior. Note, Eqn (4) can be written in the instantaneous form to relate stress and strain.

$$\mathrm{W_d} = \Delta\sigma\Delta\epsilon - 2\int_0^{\Delta\sigma} \epsilon \, \mathrm{d}\sigma \tag{5}$$

Second, it is assumed in this work that the stress ratio of $R = -1$ or the minimum stress amplitude σ_{min} is equal to $-\sigma_{\mathrm{max}}$. This equates $\Delta\sigma$ to $2\sigma_a$ where σ_a is the stress amplitude. Eqn (4) is substituted into Eqn (5) and yields Eqn (6).

$$\mathrm{W_d} = (2\sigma_{\mathrm{a}})\left(\frac{2\sigma_{\mathrm{a}}}{\mathrm{K}'}\right)^{\frac{1}{\mathrm{n}'}}\left(\frac{1-\mathrm{n}'}{1+\mathrm{n}'}\right) \tag{6}$$

Eqn (6) denotes the cyclic damaging parameter as a function of stress amplitude σ_a and our cyclic plasticity model parameters K' and n'.

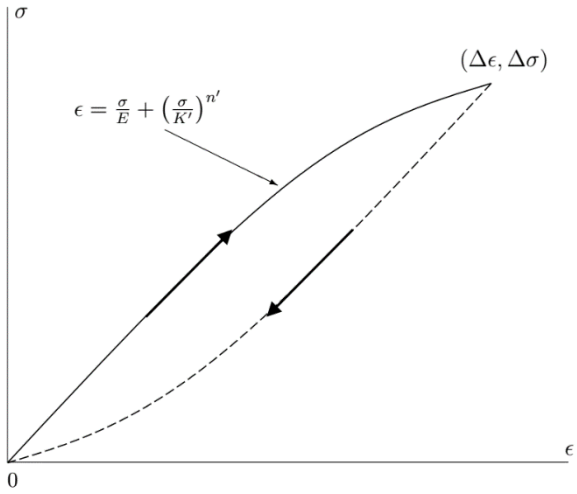

Figure 1: Fatigue Hysteresis Loop

As previously discussed from experimental finding, often W_d can be approximated as constant with good success. From previous work, this is done by finding the total strain-energy density dissipated to cause fatigue failure W_f and divided by the total cycles to failure N_f as shown in Eqn (7).

$$W_d = \frac{W_f}{N_f} \tag{7}$$

Substituting Eqn (7) into Eqn (6) and rearranging yields,

$$\mathrm{N_f} = \frac{\mathrm{W_f}}{(2\sigma_\mathrm{a})\left(\frac{2\sigma_\mathrm{a}}{\mathrm{K'}}\right)^{\frac{1}{\mathrm{n'}}}\left(\frac{1-\mathrm{n'}}{1+\mathrm{n'}}\right)} \tag{8}$$

Eqn (8) enables energy-based fatigue life prediction to occur by measuring W_f and determining the cyclic RO parameters $\mathrm{K'}$ and $\mathrm{n'}$. Like similar energy-based approaches, this can be performed experimentally and by generating data sets within the desired range of fatigue life prediction. More specifically, with $\mathrm{N_{f,i}}$, $\mathrm{W_{f,i}}$, and $\sigma_{\mathrm{a,i}}$, where i represents the test in which the data set was collected, two equations may be written from Eqn (8), and $\mathrm{n'}$ and $\mathrm{K'}$ can be solved shown in Eqn (9) and (10).

$$n' = \frac{\ln\left(\frac{\sigma_{a,1}}{\sigma_{a,2}}\right)}{\ln\left(\frac{W_{f,1}}{W_{f,2}}\frac{N_{f,2}}{N_{f,1}}\frac{\sigma_{a,2}}{\sigma_{a,1}}\right)},\ \sigma_{a,1} \neq \sigma_{a,2} \tag{9}$$

$$K' = \left[\frac{N_{f,i}}{W_{f,i}}(2\sigma_{a,i})^{\left(1+\frac{1}{n'}\right)}\frac{1-n'}{1+n'}\right]^{n'},\ i = 1\ or\ 2 \tag{10}$$

The intent of this framework is to provide a method of accelerated fatigue characterization while assuming a limited knowledge base of the material. For that reason, the Two-Point method is then utilized to generate life prediction curves using only two experimental test data sets and in a way such that the plasticity parameters $\mathrm{K'}$ and $\mathrm{n'}$ need not be assumed or found by other test methods. It is important to note here that $\left(1+\frac{1}{\mathrm{n'}}\right)$

represents the slope of a linear SN life prediction curve in log-log space and, therefore, using the Two-Point method the data must be collected at different stress amplitudes due to the mathematical derivation. Additionally, $W_{f,i}$, K', n' and represents the intercept of the SN life prediction curve. However, W_f here is used as the selection of either data set $i = 1$ or $i = 2$ to be evaluated such that life prediction curve will intercept the SN data point of $i = 1$ or $i = 2$. With K' and n' fully defined, the final life prediction curve of the Two-Point method is defined in Eqn (11).

$$N_f = \frac{W_{f,i}}{2\sigma_a \left(\frac{2\sigma_a}{K_i'}\right)^{\frac{1}{n'}} \frac{1-n'}{1+n'}} \tag{11}$$

In most situations, it is unlikely for an analysis to only be comprised of two experimental data points for fatigue life prediction. For this reason, this framework takes advantage of evaluating n', both solutions of K', and additional combinations of just two experimental data points to generate an approximate, or simulated, distribution of fatigue life curves to be later used for fatigue life prediction. It is important to note that $\forall N_f, K_i', n_i', \ni R_+$ must be rigorously enforced in Eqn (11), where all N_f, K', n' must be real and positive. If the previous condition is not satisfied, calculated K' and n' values will lead to erroneous fatigue life predictions (Celli, 2020).

Although the Two-Point method is both simple and easy to implement, the method cannot accurately capture the entire SN behavior of a material by utilizing fatigue data from only two experimental fatigue tests. This is, in part, first due to the model being insufficient to describe the discontinuity, often referred to as the "knee point", occurring in both the LCF and HCF regime in log-log space of the SN curve. Second, considerable previous work has been performed utilizing W_f, as a constant successfully but has shown systematic variation of W_f for monotonic tensile fracture and VLCF, LCF, and HCF. The method presented in this document utilizes the variation of W_f as a representation of underlying causes of fatigue behavior variation. With the implementation of stochastic approaches and Bayesian statistical inference for fatigue life prediction, the provided method can validate expected fatigue properties of a material before investing significant time and monetary investment to characterize the material.

2.2 Random Fatigue Limit Model

The RFL model, proposed by Pascual (1999), is utilized in this study and can be seen in Eqn 12.

$$\log_{10}(N_{f,i}) = \beta_0 + \beta_1 \log_{10}(\sigma_{a,i} - \gamma_i) + \epsilon_i,\ \sigma_{a,i} > \gamma_i \tag{12}$$

Where β_0 and β_1 are the model parameters and γ_i represents the endurance limit of the material. Fatigue limit, or often referred to as endurance limit, is assumed as a specified σ_a which a material can withstand an infinite number of cycles. Although a useful description, fatigue limits remain primarily an engineering approximation as most metals, with a given heat treatment, have a finite life. For this reason, the fatigue limit is viewed more as a statistical value where the probability of failure, at a given load condition, is less than a defined failure probability criterion at a defined cycle to failure criterion (e.g. 10^6) with the use of ``runouts" (Dieter, 1986). In this study, no ``runouts", or termination of fatigue test prior to failure, were collected as well as no prior fatigue limit information. This is because the intent of this work is to demonstrate the life prediction process strictly using data generated from the considered data pool. For these reasons, γ_i is assumed zero and Eqn (12) is reduced to Eqn (13).

$$\log_{10}(N_{f,i}) = \beta_0 + \beta_1 \log_{10}(\sigma_{a,i}) \tag{13}$$

2.3 Bayesian Statistical Inference

2.3.1 Bayes' Rule

In general form, Bayes' theorem is as follows in Eqn (14) where $\boldsymbol{y} = (y_1, \dots, y_n)$is a vector of n observations and $\boldsymbol{\theta} = (\theta_1, \dots, \theta_k)$ is a vector containing k model parameters (Box, 1973).

$$p(\boldsymbol{\theta} \mid \boldsymbol{y}) = \frac{p(\boldsymbol{y} \mid \boldsymbol{\theta})p(\boldsymbol{\theta})}{p(\boldsymbol{y})} \tag{14}$$

In Eqn (14), the probability of the model parameters $\boldsymbol{\theta}$ given the data set $\boldsymbol{y}$ or $p(\boldsymbol{\theta} \mid \boldsymbol{y})$, is called the posterior distribution or ``posterior'' and the desired outcome of the analysis. $p(\boldsymbol{\theta})$ is known as the prior distribution or the ``prior'' and is a representation of what is known *a priori* of the model parameters. The prior is often seen as an educated guess or represented as the initial knowledge, or lack of knowledge, of the model parameters. $p(\boldsymbol{y} \mid \boldsymbol{\theta})$ is representative of the probability of the observations $\boldsymbol{y}$ given the model parameters. However, often is the case that the the observations $\boldsymbol{y}$ are given and the parameters $\boldsymbol{\theta}$ are desired. Therefore, $p(\boldsymbol{y} \mid \boldsymbol{\theta})$ is regarded as a function of $\boldsymbol{\theta}$, rather than a function of $\boldsymbol{y}$, and written as the likelihood of $\boldsymbol{\theta}$ given $\boldsymbol{y}$ or $l(\boldsymbol{\theta} \mid \boldsymbol{y})$.

$$p(\boldsymbol{\theta} \mid \boldsymbol{y}) \propto l(\boldsymbol{\theta} \mid \boldsymbol{y})p(\boldsymbol{\theta}) \tag{15}$$

In the Bayesian approach to model calibration, there is generally an assumed prior knowledge or some prior understanding of the distribution of model parameters described with a probability distribution, mean $\mu(\theta)$ and variance $\sigma^2(\theta)$ as $P(\mu(\theta), \sigma^2(\theta))$ or as $p(\theta)$. With this in mind, Bayesian analysis is utilized in this work as it has the ability to incorporate prior knowledge or ignorance of the data as well as ``all'' or additional information (Box, 1973). Following the work performed in Celli (2019), collections of two-point energy life predictions curves from available data are used to act as prior knowledge of an estimated RFL model given the SN data observed. Thus, the prior can be described as an expected distribution or an educated guess of the parameter estimate distribution in a more systematic process.

Bayesian statistics is a powerful tool but the definition of priors remains challenging. There is a wide breadth of work as well as current research being done in this area. One often used approach that draws significant criticism outside of statistics is the use of large data sets, or the data sets themselves, to tune or define informative priors. However, this becomes a circular argument as this approach would require a large data set to analyze the phenomenon of interest when only a small data set is available. Although an effective method for curve fitting, for practical applications in situations where the data is unavailable this is not a useful process and more classical approaches are perceived to be more effective. To address this issue for fatigue analysis, a novel approach of defining priors in this work and is applied by measuring traditional SN data σ_a and N_f as well as collecting the additional of information W_f. Using the Two Point method previously described, a collection of fatigue life predictions are determined and used to simulate a population of SN experimental data. This simulated SN population is then used as the source of informative priors. The advantage of defining priors in this way enables the use of Bayesian statistics to approximate prior information sourced specifically from Two-Point method simulated data and combined with the current observed data set without the need of externally sourced information. It should be noted that this framework allows for, but does not require, the inclusion of external information, allowing for fatigue analysis in a wider breadth of situations.

A prior PDF, or simply referred to as a ``prior'', is the description of a random event with unconditional probability. That is to say, priors are representation of a belief before collected evidence or observed data is considered. However, poorly defined priors can have significant negative consequences towards data analysis and becomes a large topic of debate within the field of statistics. Bayesian Inference is therefore introduced as a method in which to characterize the inherent variance of fatigue data as well as providing a method to include prior estimated knowledge obtained from the collective Two-Point energy life predictions.

2.3.2 Model Parameter Estimation

Then with Eqn (13), fatigue life prediction process begins with a procedure similar to the work done by Babuška et al. and Douardo et al. by assuming (Babuška, 2016; Dourado, 2019) by introducing,

$$log_{10}\left(N_{f,i}^{obs}\right) = log_{10}\left(N_{f,i}^{model}\right) + \epsilon_i \tag{16}$$

Note that $\log_{10}\left(\mathrm{N}_{\mathrm{f,i}}^{\mathrm{model}}\right)$ is represented by Eqn (16) and ϵ_i is the observation error. ϵ is assumed i.i.d and constant variance $\epsilon \sim \mathrm{N}(\mu = 0, \lambda = \mathrm{Cte})$. Given the sample data $\mathrm{N_f} = \left(\mathrm{N_{f,1}}, \ldots, \mathrm{N_{f,m}}\right)$, the likelihood function is then written as

$$l\left(\sigma_a^{obs}, \theta, \lambda \mid N_f^{obs}\right) = \prod_{i=1}^{m} \frac{1}{(2\pi\lambda)^{\frac{1}{2}}} exp\left(-\frac{\epsilon_i^2}{2\lambda}\right) \tag{17}$$

Finally, identifying that we are only interested in the proportionality of the posterior we ignore the denominator and rewrite Eqn (15) as,

$$\mathrm{p}\left(\sigma_\mathrm{a}^{\mathrm{obs}}, \theta, \lambda \mid \mathrm{N_f^{obs}}\right) \propto \mathrm{l}\left(\sigma_\mathrm{a}^{\mathrm{obs}}, \theta, \lambda \mid \mathrm{N_f^{obs}}\right) \mathrm{p}(\theta)\mathrm{p}(\lambda) \tag{18}$$

Note that the model parameters are assumed to have a normal distribution and the variance is assumed to have an inverse gamma prior distribution $\mathrm{p}(\lambda)$.

2.3.3 Bayesian Update

With each unique life prediction from Eqn (11) is calculated over a specified range $\sigma_\mathrm{a}^{\mathrm{predic}}$. This range is defined in order to encompass the range from LCF to the highest desired cycle count to be analyze.

- **Compute** n', K_i' for each σ_a^{obs} pair using Eqn 9 and 10.
- **Define** a discrete interval of $\sigma_a^{range} = \left(\sigma_{a,max}, \ldots, \sigma_{a,min}\right)$ where the stress amplitude considered falls within the range of $\left(\sigma_{a,max} > \sigma_{a,i} > \sigma_{a,min}\right)$. Note, σ_a^{range} is initially approximated by the user to produce SN data over the desired cyclic failure range of interest. Therefore, the bound of σ_a^{range} may be approximated using the initial predictions from Eqn (11) or inspection of SN behavior of like materials. In this study, $\sigma_a^{range} = \left(\sigma_a\left(N_f = 10^1\right), \ldots, \sigma_a\left(N_f = 10^7\right)\right)$ and is defined with a length equivalent to the number of SN data points considered for determining K' and n'
- **Compute** $N_{f,i}^{predic}$ from the Two-Point method as a function of $f\left(\sigma_{amp,i}^{obs}, \mathrm{W}_{f,i}\right)$ for the pair of experimental tests i.
- **Apply** least squares regression (LSR) to estimate model parameter prior distribution
  - $\beta_0 \sim \mathrm{N}\left(\mu\left(\beta_0^{2\mathrm{pt}}\right), \sigma^2\left(\beta_0^{2\mathrm{pt}}\right)\right)$
  - $\beta_1 \sim \mathrm{N}\left(\mu\left(\beta_1^{2\mathrm{pt}}\right), \sigma^2\left(\beta_1^{2\mathrm{pt}}\right)\right)$
  - $\epsilon \sim \mathrm{N}(0, \sigma^2)$ where $\sigma^2 \sim \mathrm{IG}(\alpha^{2\mathrm{pt}}, \beta^{2\mathrm{pt}})$ and α and β are the shape and scale parameters of the inverse gamma distribution respectively.

- **Define** the prior distribution as the probability of the model parameters $p_0(\beta_0)$, $p_1(\beta_1)$, and $p_2(\sigma^2)$.

- **Compute** the maximum distributions, such as Monte Carlo Markov Chains. In this study, Gibbs Sampler is used to generate posterior samples, with 10000 samples generated with a burn-in period of 5000 samples, and determine posterior MLE.posterior estimates from Eqn (18). Note, a variety of algorithms are used for sampling from probability

- **Update**, after the first Bayesian update p_0, p_1, p_2 as a weighted sum from the Two-Point method defined as $p_i = wp_i^{\text{Two-Point}} + (w-1)p_i^{\text{prev.post.}}$. The weighted value w is defined by the user and represents the level of credibility associated with each prior. In this work, w is assigned as 0.5 for consistency and using the previous step's empirical mean and standard deviation from the posterior distribution of RFL model parameters.

Note that the superscript ``2pt" simply denotes the model parameters determined only from N_f^{predic} at σ_a^{obs}.

3.0 EXPERIMENTAL PROCEDURE

All axial fatigue tests were conducted on an MTS servo-hydraulic load frames. An MTS FlexTest 60 was used for both test control and data acquisition of time, load, and strain signals. Strain measurements were collected via an MTS axial extensometer. For EBM Ti 6Al-4V, strain data was collected using digital image correlation (DIC).

The MTS 661.20E-03 load cells and linear variable differential transducers (LVDT) were previously certified, performed annually, and calibrated following ASTM standards and MTS guidance prior to testing. Extensometers, were properly calibrated following vendor guidance and strain measurements were verified not to exceed 0.5% error with an MTS Extensometer Calibrator 650.03 and following ASTM E83.To ensure proper alignment prior to testing, an alignment procedure was conducted with an MTS 609 alignment fixture, installed on all servo-hydraulic load frames, and used in conjunction with MTS Easy Alignment hardware and software. This was done to ensure an ASTM E1012 Class 5 throughout testing.

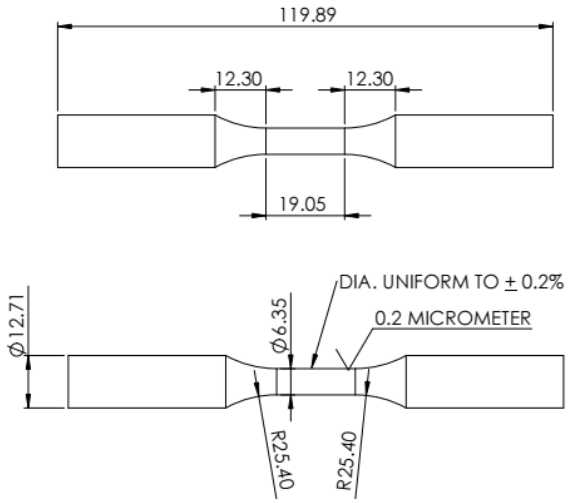

Figure 2: AL6061-T6 Round Dogbone Specimen.

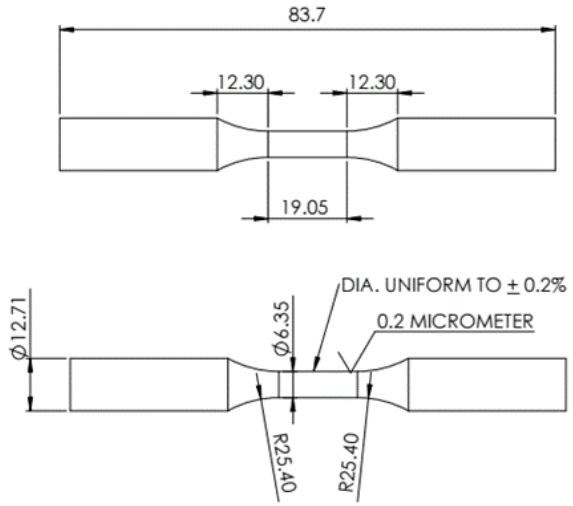

Figure 3 DMLS IN718 and EBM Ti 6Al-4V Round Dogbone Specimen.

For DIC experiments, a full field of view was required for optical strain information, and available extensometer attachments obstructed key measurement locations along the gage length of the specimen. For this reason, extensometery was not used except during tensile testing to validate DIC post-processing parameters and strain measurements. The practice of monitoring fatigue damage and validating DIC measurements of cyclic SED as a substitute to extensometery has been previously performed in an earlier study conducted by Celli (2019).

DIC was performed with a stereo camera rig, or two cameras attached to the same bar or fixture, assumed rigid. The cameras were both GS3-U3-123S6M-C FLIR Grasshopper3 HRDC with 12.3 MP resolution and Schneider XNP 1.9/35-0901 lenses set with a f# of 8. The cameras had a stereo angle of 22.5° and a working distance of 67.5mm. The magnification of the cameras resulted in averaged 60.9 pixels per mm. High intensity flood lights were used to illuminate the specimen and allow for a reduction in exposure time. The exposure time across all tests were on the order of 5ms; however, the exposure time was adjusted for each fatigue test to ensure the most desirable contrast was obtained.

The image acquisition was controlled through Correlated Solutions Vic-Snap 8 software. Fatigue test frequency and image acquisition was varied to ensure a proper measurement of hysteresis energy could be made. With a camera frame rate of 5 Hz, the frequency of the fatigue test during image acquisition was set to 0.07 Hz for two cycles. This was done to collect approximately 72 images per cycle and to adequately resolve the hysteresis loop for an energy measurement. The test frequency was then changed to a higher test frequency.

4.0 RESULTS

4.1 Aluminum 6061-T6

The overall accumulated AL6061-T6 data can be seen in Figure 4. Al6061-T6 Data collected by Celli (2020), and Holycross (2016) are represented by filled in markers denoting SED data was also collected with SN data and SED data. HCF and VHCF data collected by Scott-Emuakpor (2016) and Yahr (1993) is also presented in Figure 4 indicated by hollow triangular markers. The SN data that includes companion SED data is used in conjunction with the methodology described in this paper for HCF life prediction with LCF data and the SN data without companion SED data is used as a validation data set.

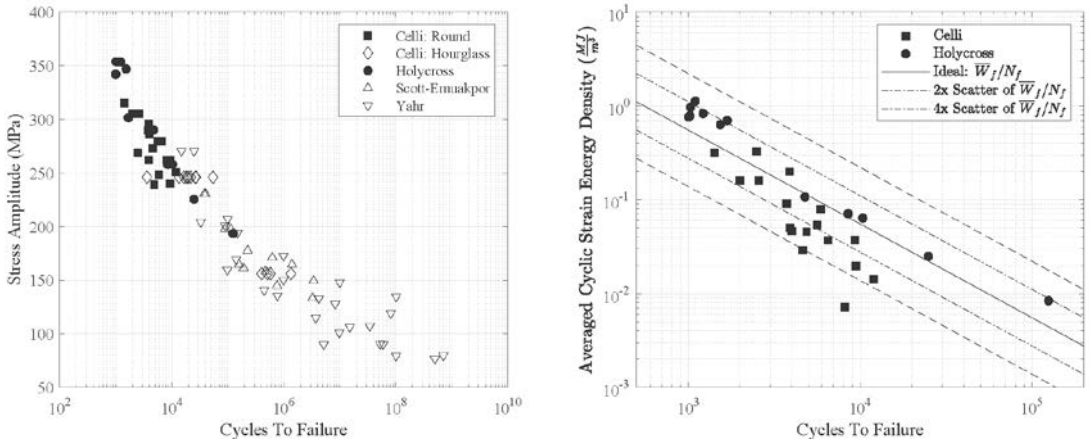

Figure 4: AL6061-T6 (Left) SN Curve and (Right) Cyclic SED Data.

The comparisons of the fatigue life prediction with respect the LSR considering all the data, the reduced data set, and Two-Point MCM method is presented in Figure (5) with 5, 15, and 29 experimental tests considered, respectively. The solid black circular markers represent the reduced data set considered, the solid grey circular markers represent the censored or remaining SN data with corresponding SED data not considered, and the hollow black circular markers represent the rest of the data found either experimentally or from literature. This comparison demonstrates graphically the utility of accurately predicting LCF fatigue life as well as forecasting HCF behavior by deploying the developed hybrid Two-Point BSI life prediction algorithm. Furthermore, comparative analysis of the Two-Point BSI framework to that of the LSR of the reduced data set in Fig. (5) shows that the hybrid Two-Point BSI is a better approximation for the RFL model parameters. These figures again demonstrate graphically the Two-Point BSI method converges towards the LSR considering all the data quickly with only 5, or 10, SN points and with 29 SN points or more the figure is nearly identical. As a quantitative metric, the analysis of the root mean squared error (RMSE), in Table 1, of the forecasted prediction again shows significantly better performance of the Two-Point BSI method when compared to the LSR of the reduced data.

As a comparison considering experimental effort, the total test duration for the reduced data set considering 5, 10, 15, 20, 25, and 29 experimental tests would take 0.5, 0.8, 1.5, and 3.8 hours of experimental testing time at a test frequency of 20Hz. If one considers the length of time to generate the presented data at 10^7 cycles to failure or less at the same test frequency it would take 643 hours or 26.8 days of continual testing. If one then considers all the data, the total testing time would be 23815 hours or approximately 2.8 years. Although the latter is an extreme example and would likely require different experimental techniques, including ultrasonic fatigue testing, this exemplifies how utilizing the Two-Point Test method can reduce experimental testing time by 99.4 to 99.8% for 10^7 cycles to failure or less.

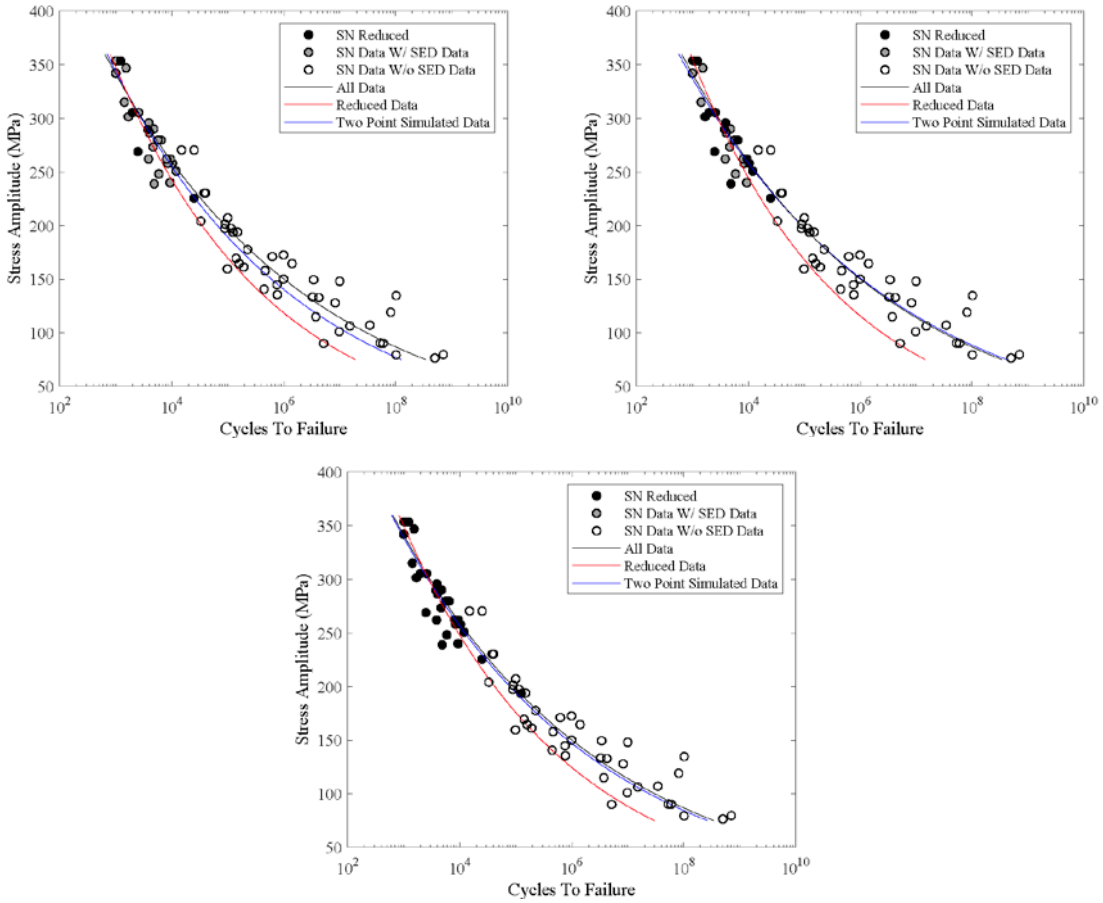

Figure 5: AL6061-T6 SN Life Prediction with 5 (Top-Left), 10 (Top-Right), and 29 (Bottom) Experiments.

Table 1: AL6061-T6 Forecast RMSE.

Exp. Tests	Reduced Data	Two-Point BSI
5	0.914	0.587
10	0.798	0.514
15	0.957	0.512
20	0.965	0.512
25	0.970	0.521
29	0.812	0.520
All Data: 0.510		

4.2 DMLS Inconel 718

DMLS IN718 fatigue tests were performed to demonstrate the utility of the Two-Point BSI life prediction framework. With particular emphasis, the life prediction of IN718 is intended to show the application of the proposed method to forecast fatigue behavior of AM materials. IN718 is of high interest to the aerospace community and has become a common selection for both material powder to print as well as additional forms for other additive processes to manufacture aerospace components such as turbine blades. The fatigue data is presented graphically in Fig. 6.

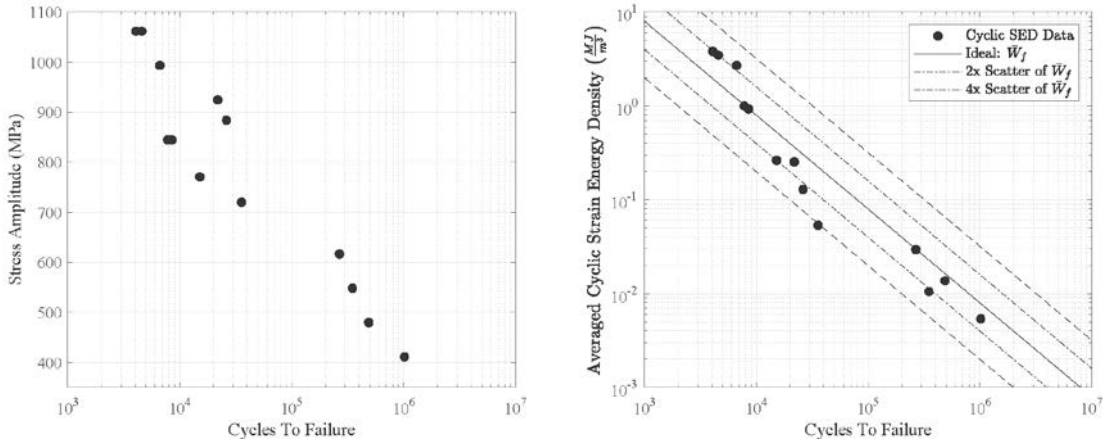

Figure 6: DMLS IN718 (Left) SN Curve and (Right) Cyclic SED Data.

The experimentally found SN curve of IN718 presents a clear linear trend in SN with slight variation between the stress amplitudes of 700 and 900 MPa. From Figure 6, the SED data does not directly correspond to the same variation trend in the SN data. Although cyclic SED was collected, data exceeding 10^6 cycles to failure is censored in the framework to provide an example case in which the method could be used to forecast HCF SN data with LCF data.

Despite the variation seen with the introduction of experimental tests, the model parameters begin to converge but likely need additional experimental tests to ensure convergence. Analysis of the RMSE, seen in Table 2, of the forecasted prediction again shows significantly better performance of the Two-Point BSI method when compared to the LSR of the reduced data. The resulting life prediction curves can be seen in Figure 7.

Table 2: DMLS IN718 Forecast RMSE.

Exp. Tests	Reduced Data	Two-Point BSI
4	0.504	0.330
5	0.746	0.295
6	0.589	0.378
7	0.497	0.246
8	0.585	0.220
9	0.576	0.258
All Data: 0.202		

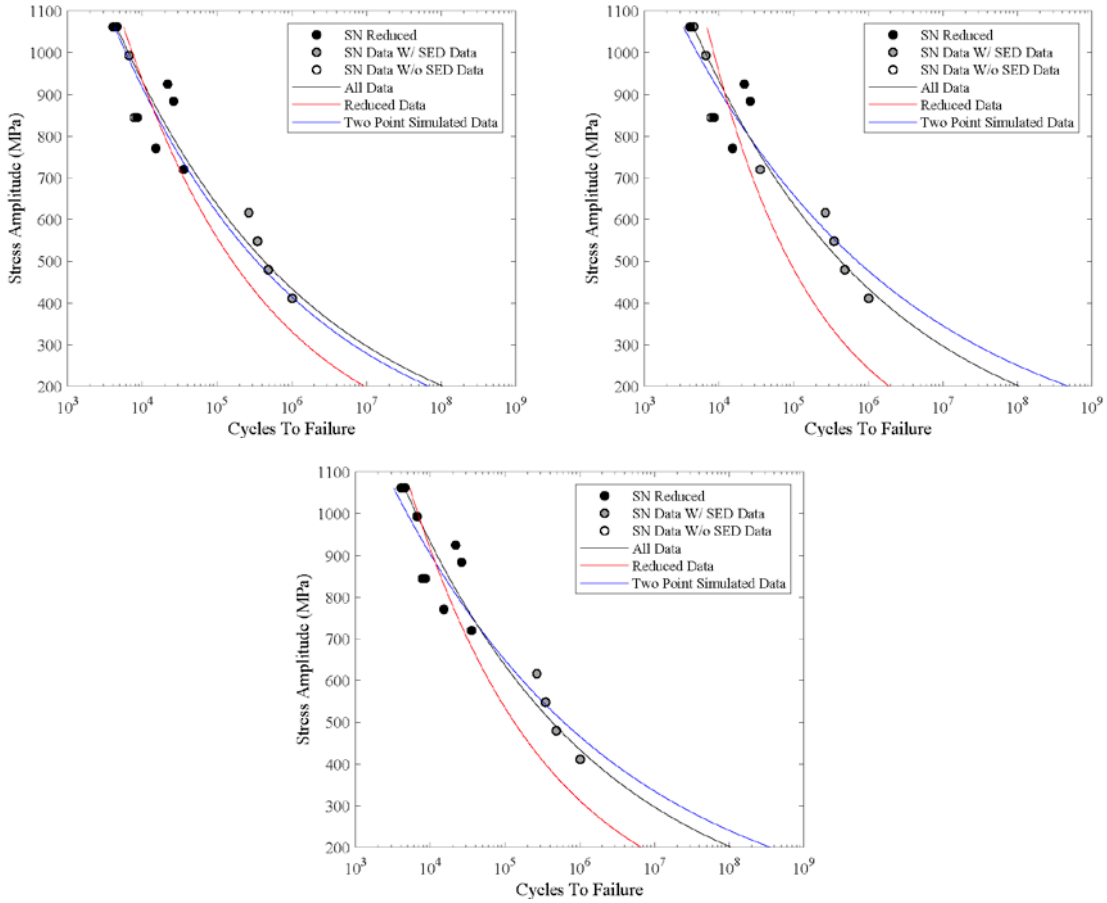

Figure 7: DMLS IN718 SN Life Prediction with 5 (Top-Left), 7 (Top-Right), and 9 (Bottom) Experiments.

4.2 EBM Ti 6Al-4V

The Two-Point BSI framework is applied to EBM Ti 6Al-4V as the second AM material considered to demonstrate the utility of the approach. The SN data and cyclic SED data can be seen in Figure 8. Figure 8 shows the SN data following an approximately linear trend. Only one SN data point does not have corresponding SED data. From Figure 8, each specific data set appears to follow its own linear trend. However, it was found experimentally, for some cases, a crack had initiated almost immediately at the onset of the fatigue test. It is suspected that sub-optimal process parameters during the EBM caused large volumetric defects throughout the material in some cases but not consistently throughout the population of specimens. An example of this can be seen in Figure (9) and (10). The presence of such features increase the magnitudes of strain concentrated at the local defects. In turn, the use of extensometers, whether physical or virtual, would no longer provide an accurate representation of strain or damage as the normal strain field is no longer uniform throughout the gauge section. For this reason, the cyclic SED data reported in Figure (8) is censored and was not incorporated into the Two-Point fatigue life prediction framework due to the violated assumption of a uniform strain field to measure cyclic SED.

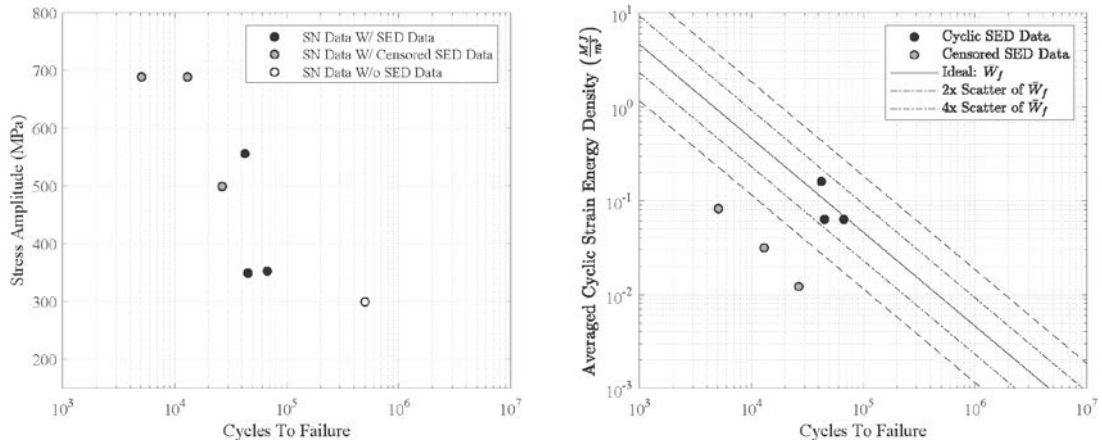

Figure 8: EBM Ti 6Al-4V (Left) SN Curve and (Right) Cyclic SED Data.

Figure (9) reveals a large void due to lack of fusion with partially fused powder as the point of crack initiation as well as a significant number of other lack of fusion locations detected along the surface. Post mortem inspection via DIC measurements revealed higher localized strain at the location of crack initiation almost immediately after the onset of the test. In contradiction, virtual extensometer measurements, encompassing the gauge section, revealed an approximately consistent strain amplitude but smaller plastic strain response. Therefore, it is hypothesized that the assumption of the SED measurement, uniform damage throughout the volume of the material, is invalid and thus censored from analysis.

In contrast to the large void specimens, Figure (10) shows small locations of lack of fusion on the fracture surface. Virtual extensometer as well as a point measurement, placed at the location of fatigue rupture, each gathered data that calculated cyclic SED, of 0.185 $\frac{\mathrm{MJ}}{\mathrm{m}^3}$ and 0.183 $\frac{\mathrm{MJ}}{\mathrm{m}^3}$, respectively, approximately 1.5% difference. Therefore, the Two-Point fatigue life prediction can be applied to the data points associated with these specimens.

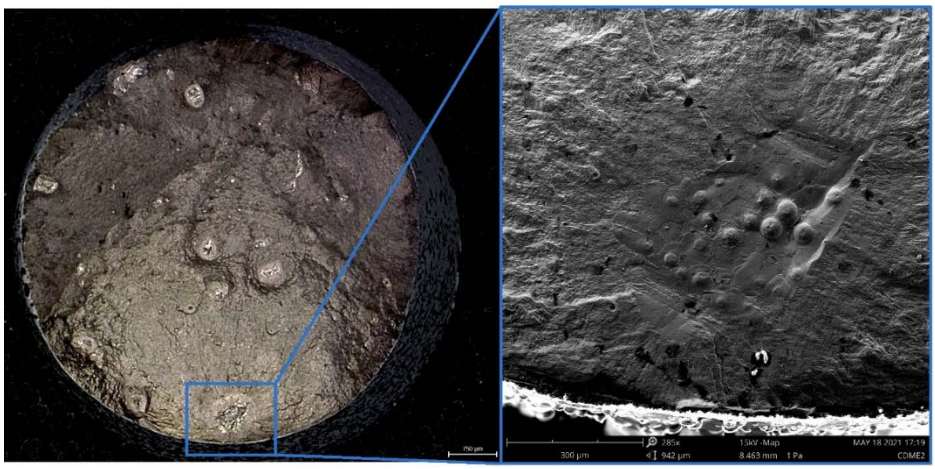

Figure 9: LCF EBM Ti 6Al-4V.

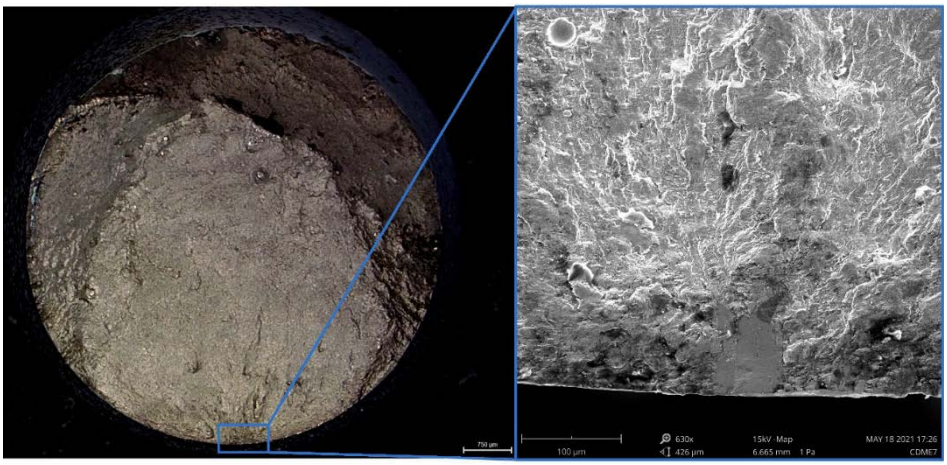

Figure 10: HCF EBM Ti 6Al-4V.

Table 3 presents the RMSE of the forecasted data and the life predictions for EBM Ti 6Al-4V are presented in Figure (11). Although one point is considered in this case, the Two-Point BSI method interestingly outperforms the LSR of the reduced data set even as it converges towards the all-data fit. However, from observation of the life predictions the slope of the Two-Point BSI is steeper than that of the reduced data set when considering 5 and 6 experimental tests. For this reason, with the inclusion of additional HCF data, it would then be suspected that the LSR considering all the data would outperform the Two-Point BSI method. It can be seen that the Two-Point BSI method initially is a closer representation of the All data LSR when compared to the Reduced data set. However, with the introduction of additional points the LSR of the reduced data set converges more closely to that of the LSR of all the data. This remains unsurprising as additional SED information is not being provided to the Two-Point BSI method as the data is censored. Of note, using DIC in conjunction with the Two-Point BSI method demonstrates the capability to identify underlying phenomena separating specimens within the sample population.

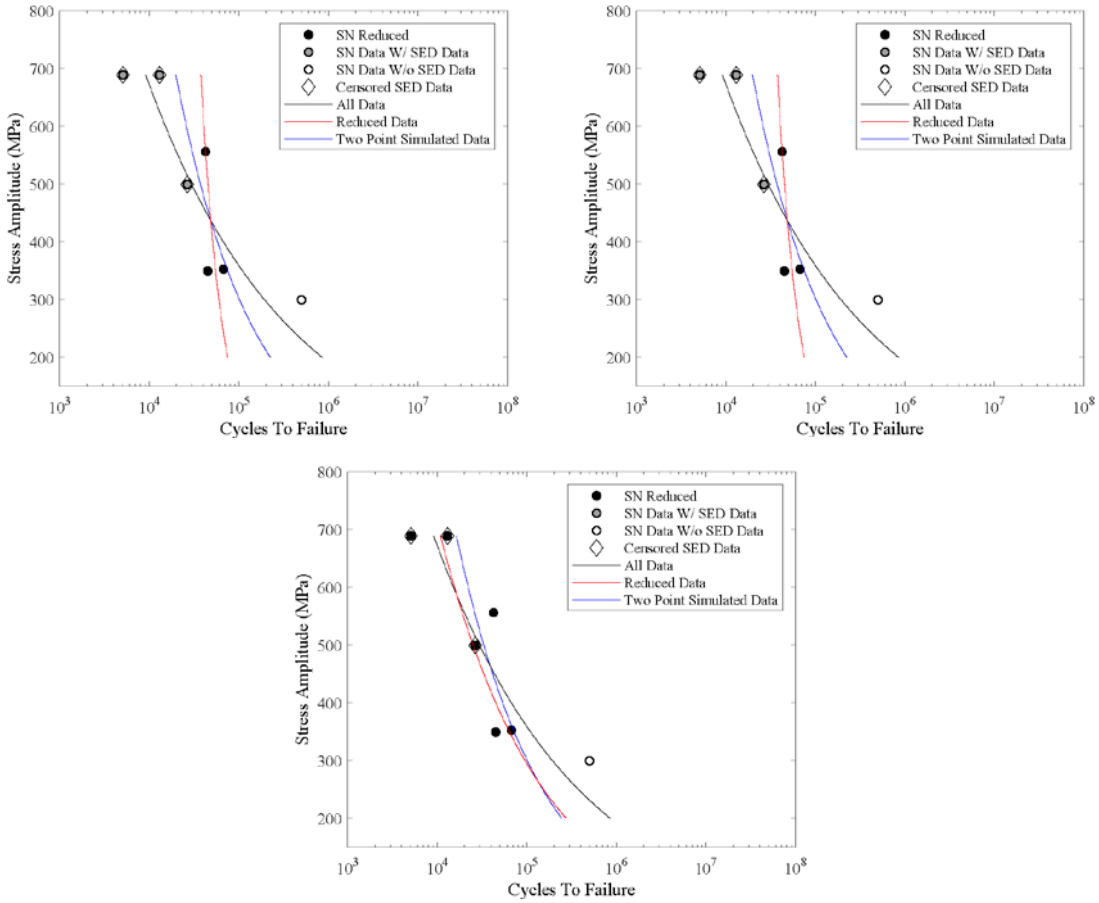

Figure 11: EBM Ti 6Al-4V SN Life Prediction with 3 (Top-Left), 5 (Top-Right), and 6 (Bottom) Experiments.

Table 3: EBM Ti 6Al-4V Forecast RMSE.

Exp. Tests	Reduced Data	Two-Point BSI
3	0.921	0.692
4	0.703	0.695
5	0.724	0.694
6	0.719	0.694
All Data: 0.412		

5.0 CONCLUSION AND FUTURE WORK

The proposed framework first utilizes a simplistic Two-Point life prediction to generate multiple life prediction curves that were then used to approximate the variation of fatigue life against repeated stress fatigue tests successfully. Then, the method was combined with stochastic sampling techniques of Monte Carlo simulation as well as Bayesian Statistical Inference to evaluate common SN curve models used within the literature, specifically the random fatigue limit model. The proposed method has demonstrated the ability to approximate and forecast SN fatigue life while reducing the total experimental testing time by 99.4 to 99.8%. The life prediction framework presented in this document provides a highly efficient tool for the investigation of prediction of fatigue life and variability of fatigue life concurrently and rapidly for investigation of candidate AM materials and associated process parameter.

REFERENCES

Atzeni, E. & Salmi, A. (2012), 'Economics of additive manufacturing for end- usable metal parts', International Journal of Additive Manufacturing Technologies 62(9), 1147–1155.

Babuška, I., Z., S., Scavino, M., Szab´o, B. & Tempone, R. (2016), 'Bayesian Inference and Model Comparison for Metallic Fatigue Data', Computer Methods in Applied Mechanics and Engineering 304(1), 171–196.

Box, G. & Tiao, G. (n.d.), Bayesian Inference in Statistical Analysis, Addison- Wesley Publishing Company.

Celli, D. (2017), Measurement of Hysteresis Energy Using Digital Image Correlation with Application to Energy Based Fatigue Life Prediction and Assessment, Thesis, The Ohio State University.

Celli, D. (2017), Measurement of Hysteresis Energy Using Digital Image Cor- relation with Application to Energy Based Fatigue Life Prediction and Assessment, Thesis, The Ohio State University.

Celli, D., Shen, H., Holycross, C., Scott-Emuakpor, O. & George, T. (2019), 'Measurement of Hysteresis Energy Using Digital Image Correlation With Application to Energy-Based Fatigue Life Prediction', Journal of Engineering for Gas Turbines and Power 141(9).

Celli, D., Shen, H., Scott-Emuakpor, O., Holycross, C. & George, T. (2020), 'Stochastic Fatigue Life Prediction Based on a Reduced Data Set', Journal of Engineering for Gas Turbines and Power 142(3).

Dieter, G. (1986), Mechanical Metallurgy, McGraw-Hill.

Dourado, A., Irmak, F., Viana, F. & Gordon, A. (2019), A Bayesian Framework for Estimation of Strain Life Lower Bounds and its Application to IN617, in 'ASME Turbo Expo', Phoenix Arizona, pp. GT2019–91958.

Enomoto, N. (1955), 'On Fatigue Tests Under Progressive Stress', American Society for Testing Materials 55, 903–917.

Feltner, C. E. & Morrow, J. D. (1961), 'Microplastic Strain Hysteresis Energy as a Criterion for Fatigue Fracture', Journal of Basic Engineering pp. 15–22.

Holycross, C., Shen, H., Scott-Emuakpor, O. & George, T. (2015), 'Energy- Based Fatigue Life Prediction For Combined Low Cycle And High Cycle Fatigue Regimes', The Journal of Strain Analysis for Engineering Design 50(2).

Holycross, C. (2016), A multiscale analysis and extension of an energy-based fatigue life prediction method for high low and combined cycle fatigue., Dissertation, The Ohio State University.

Jared, B., Boyce, B., Madison, J., Rodelas, J. & Salzbrenner, B. (2015), 'Defect Characterization for Material Assurance in Metal Additive Manufacturing'.

Jasper, T. M. (1923), 'The Value of the Energy Relation in the Testing of Ferrous Metals at Varying Ranges of Stress and at Intermediate and High Temperatures', The London, Edinburgh and Dublin Philosophical Magazine and Journal of Science 46(274), 609–627.

Leino, M., Pekkarinen, J. & Soukka, A. (2016), 'The role of laser additive manufacturing methods of metals in repair, refurbishment and remanufacturing - enabling circular economy', Physics Procedia 83, "752–760".

Machin, A. S. (1984), 'Structures technical memorandum 371 how many specimens - an aid in the design of fatigue test programs', Department of Defence, Defence Science and Technology Organisation Aeronautical Research Laboratories.

Mani, M., Lane, B., Donmez, A., Feng, S., Moylan, S. & Fesperman, R. (2015), Measurement Science Needs For Real-Time Control of Additive Manufacturing Powder Bed Fusion Processes, National Institute of Standards and Technology.

Optomec (2015), 'Optomec customers surpass 10 million turbine blade repairs using metal AM'. https://optomec.com/optomec-customers-surpass-10-million- turbine-blade-repairs/. Accessed: 2021-04-07.

Ozaltun, H., Seidt, J. D., Shen, M.-H. H., George, T. J. & Cross, C. J. (2009), An Energy-based Method for Uni-axial Fatigue Life Calculation, in 'Proceedings of 2009 ASME/IGTI Turbo Expo', Orlando, pp. 1–8.

Pascual, F. & Meeker, W. (1999), 'Estimating Fatigue Curves With the Random Fatigue-Limit Model', Technometrics 41(4), 277–289.

Raju, R., Duraiselvam, M., Petley, V., Verman, S. & Rajendran, R. (2015), 'Microstructural and mechanical characterization of Ti6Al4V refurbished parts obtained by laser metal deposition', Material Science and Engineering: A 643, "64–71".

Salem, A., Beuth, J., Harrysson, O. & Lewandowski, J. (2016), 'Overview of Materials Qualification Needs for Metal Additive Manufacturing', The Journal of The Minerals, Metals and Materials Society 68(3), 747–764.

Schneider, C. R. A. & Maddox, S. J. (2003), 'Best practice guide on statistical analysis of fatigue data', International Institute of Welding.

Shen, M. H. & Akanda, S. (2015), 'An energy-based approach to determine the fatigue strength and ductility parameters for life assessment of turbine materials', Journal of Engineering for Gas Turbines and Power 137(7).

Shen, M. & Akanda, S. (2016), 'A modified closed form energy-based framework for fatigue life assessment for aluminum 6061-T6: Strain range approach', International Journal of Damage Mechanics 25(5), 875–880.

Scott-Emuakpor, O., George, T., Cross, C. & Shen, M.-H. (2004), 'Development of an Improved High Cycle Fatigue Criterion', Journal of Engineering for Gas Turbines and Power 129(1), 162–169.

Scott-Emuakpor, O. E., Shen, M.-H. H. & Cross, C. J. (2007), 'Development of an Improved High Cycle Fatigue Criterion', Transactions of the ASME 129, 162–169.

Scott-Emuakpor, O., George, T., Cross, C., Wertz, J. & Shen, M.-H. H. (2010), Validation of a Multi-Axial Fatigue Life Prediction using Maximum Shear Experimental Results, in '2010 ASME Turbo Expo: Power for Land, Sea & Air', Glasgow, pp. 1–8.

Scott-Emuakpor, O., George, T., Holycross, C., Brown, J., & Beck, J. (2016), Fatigue Behavior Comparison Between Ultrasonic and Servohydraulic Axial Testing Procedures., in '2016 ASME Turbo Expo, Seoul, North Korea, GT2016-56387

Scott-Emuakpor, O., Runyon, B., George, T., Goldin, A., Holycross, C., Sheridan, L., Langley, B., Gillaugh, D., Kannan, M., Shresta, S. & Gyekenyesi, A. (2021), Structural Integrity Assessments for Validating Directed Energy Deposition Repairs of Integrally Bladed Rotor, in 'ASME Turbo Expo', Virtual Online. GT2020-14361.

Stowell, E. Z. (1969), 'Theory of Metal Fatigue at Elevated Temperatures', Nuclear Engineering and Design 9, 239–257.

Thomas, D. & Gilbert, S. (2014), Costs and Cost Effectiveness of Additive Manufacturing 1176, Technical report, U.S. Department of Commerce, National Institute of Standards and Technology.

Verma, R. & Kaushal, G. (2019), 'State of the Art of Powder Bed Fusion Additive Manufacturing: A Review', 3D Printing and Additive Manufacturing Technologies pp. 269–279

Yahr, G. T., Fatigue Design Curves for 6061-T6 Aluminum. (1993) U.S. Web. Doi:10.1115/1.2842286